JOURNAL OF APPLIED PHYSICS **116**, 224302 (2014)

Measuring the depth profiles of strain/composition in AlGaN-graded layer by high-resolution x-ray diffraction

A. V. Kuchuk,[1,2] H. V. Stanchu,[2] Chen Li,[1] M. E. Ware,[1] Yu. I. Mazur,[1] V. P. Kladko,[2] A. E. Belyaev,[2] and G. J. Salamo[1]

[1]*Institute for Nanoscience & Engineering, University of Arkansas, W. Dickson 731, Fayetteville, Arkansas 72701, USA*

[2]*V.Lashkaryov Institute of Semiconductor Physics, National Academy of Sciences of Ukraine, Pr. Nauky 45, Kyiv 03028, Ukraine*

(Received 22 August 2014; accepted 2 December 2014; published online 12 December 2014)

Here, we demonstrate X-ray fitting through kinematical simulations of the intensity profiles of symmetric reflections for epitaxial compositionally graded layers of AlGaN grown by molecular beam epitaxy pseudomorphically on [0001]-oriented GaN substrates. These detailed simulations depict obvious differences between changes in thickness, maximum concentration, and concentration profile of the graded layers. Through comparison of these simulations with as-grown samples, we can reliably determine these parameters, most important of which are the profiles of the concentration and strain which determine much of the electrical properties of the film. In addition to learning about these parameters for the characterization of thin film properties, these fitting techniques create opportunities to calibrate growth rates and control composition profiles of AlGaN layers with a single growth rather than multiple growths as has been done traditionally.
© *2014 AIP Publishing LLC*. [http://dx.doi.org/10.1063/1.4904083]

I. INTRODUCTION

Group III-nitride alloys, $Al_xGa_{1-x}N$, are finding more and more practical applications in modern optoelectronic devices. Recently, increased interest in the study of compositionally graded $Al_xGa_{1-x}N$ layers has surged due to their unique properties. There have been recent demonstrations of p-type doping and doping enhancements through the so-called polarization doping technique resulting from grading the composition of III-nitride alloys.[1–4] In addition to simple demonstrations of high doping levels, there have been studies of improved p-type ohmic contacts and tunnel junctions,[5] as well as demonstrations of new types of deep-UV (ultraviolet) light emitters (LEDs and lasers).[5–9] Moreover, there have been further demonstrations that compositionally graded $Al_xGa_{1-x}N$ may also serve as strain transition buffer layers and dislocation filters for the growth of crack-free GaN on Si(111) substrates.[10–12]

The depth profile of the aluminum content is the key factor in modifying the properties of graded $Al_xGa_{1-x}N$ layers. Thus, a crucial issue in the growth of these layers is the precise control of the Al flux so that the composition changes controllably with depth. Various modes have been employed to affect the flux of material on a substrate in molecular beam epitaxy (MBE). In Refs. 1, 2, and 7, the Al cell temperature (T_{Al}) was changed logarithmically in order to achieve a linear grade of composition. In Ref. 8, both Al and Ga effusion cells temperatures were ramped logarithmically to achieve a linear grade while maintaining a stoichiometric relationship between the metal and the nitrogen flux. And, in Ref. 9 a shutter pulsing technique was used to control the grade of the film. However, there are further complications that must be considered: (a) The effusion cell temperature has a finite settling time after a temperature change and consequently the Al flux depends not only the temperature but the ramping rate as well. (b) The Al flux cannot in most cases be accurately measured in real-time during growth. And, (c) effusion cell fluxes have time dependent instabilities for many reasons,[13] including shutter transients, depletion of source materials, and secondary phase formation on the surface of the hot metal source material. Therefore, process control requires rapid and reliable characterization of depth profiles of chemical composition and strain in graded $Al_xGa_{1-x}N$ layers.

X-ray diffraction (XRD) is a nondestructive technique that permits rapid determination of the chemical composition, strain state, and thickness of epitaxial layers. The chemical composition and strain are extracted from accurate measurements of the in-plane and out-of-plane lattice parameters. Several techniques[14–16] have been proposed to measure the composition and strain in non-graded $Al_xGa_{1-x}N$ layers. In this study, we extend the XRD method to the case of graded $Al_xGa_{1-x}N$ layers. We study a method based on a laboratory X-ray diffraction experiment, which allows for differentiation between different Al depth profiles in graded $Al_xGa_{1-x}N$ layers. Moreover, we compare simulated and experimental data for graded $Al_xGa_{1-x}N$ layers grown by plasma-assisted MBE. Finally, we show how to use the simulated data for calibration of the Al cell temperature for the growth of general $Al_xGa_{1-x}N$ layers.

II. THE SIMULATION PROCEDURE

Because both strain and chemical composition affect the in-plane and out-of-plane lattice parameters of $Al_xGa_{1-x}N$ epitaxial films, the standard approach to determine both quantities is to measure a symmetric and an asymmetric X-ray reflection in the $2\theta/\omega$ configuration. The interplanar

 © 2014 AIP Publishing LLC

[This article is copyrighted as indicated in the article. Reuse of AIP content is subject to the terms at: http://scitation.aip.org/termsconditions. Downloaded to] IP: 193.17.216.226 On: Tue, 16 Dec 2014 12:31:26

spacing, d_{hkl}, is calculated from Bragg's law, $n\lambda = 2d_{hkl}\sin(\theta)$, where n is the diffraction order; λ is the wavelength of the incident X-rays; θ is the scattering angle; and (h, k, l) are the Miller indices of the diffracted plane. The a and c lattice parameters are then found from the interplanar spacing equation for hexagonal crystals given by

$$\frac{1}{d^2} = \frac{4(h^2 + hk + k^2)}{3a^2} + \frac{l^2}{c^2}. \tag{1}$$

First, the c lattice parameter is determined from a symmetric $(h = k = 0)$ reflection. Then using that c, the a lattice parameter is determined from an asymmetric (h, k, l) reflection. After the in-plane and out-of-plane lattice parameters of the layer are precisely determined, the composition and strain of the $Al_xGa_{1-x}N$ layer can be determined assuming biaxial strain and Vegard's law. The in-plane ($\varepsilon_{\parallel} = \frac{a(x)-a_r(x)}{a_r(x)}$) and out-of-plane ($\varepsilon_{\perp} = \frac{c(x)-c_r(x)}{c_r(x)}$) strain for the wurtzite structure are related by the following equation for biaxial strain:

$$\varepsilon_{\perp} = -2\frac{C_{13}(x)}{C_{33}(x)}\varepsilon_{\parallel}, \tag{2}$$

where $C_{13}(x)$ and $C_{33}(x)$ are the elastic constants of the alloy. All of the constants for fully relaxed $Al_xGa_{1-x}N$, $a_r(x)$, $c_r(x)$, $C_{13}(x)$, and $C_{33}(x)$, vary with the composition, x_{Al}. In general, this is assumed to be linear resulting in Vegard's law stated as

$$A^{Al_xGa_{1-x}N} = xA^{AlN} + (1-x)A^{GaN}, \tag{3}$$

where A^{AlN} and A^{GaN} represent each constant in the AlN and GaN bulk crystal, respectively. Finally, combining Eqs. (2) and (3) along with the definitions for in- and out-of-plane strain, the composition and strain state can be uniquely determined.

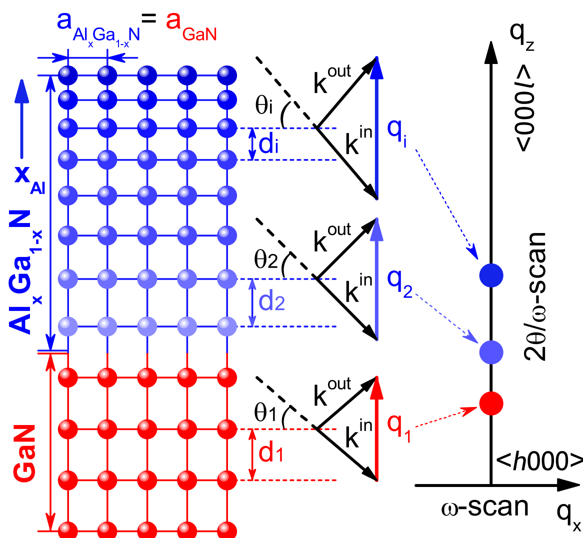

FIG. 1. Pseudomorphic growth illustration of graded $Al_xGa_{1-x}N$ on [0001]-oriented GaN demonstrating how the diffracted intensity is distributed in reciprocal space from the different sub-cells. d_i is the interplanar spacing as a function of $Al_xGa_{1-x}N$ for sub-cell i; θ_i is the Bragg angle for ith sub-cell; and q_i are the scattering vectors that correspond to each diffraction condition.

For graded $Al_xGa_{1-x}N$ layers, the situation is a little different. As can be seen from Fig. 1 which depicts graded $Al_xGa_{1-x}N$ coherently strained to a GaN substrate, the Al composition affects only the out-of-plane lattice parameter. Thus, for pseudomorphic growth we have a distribution of only the out-of-plane lattice parameter, $c \sim f(x_{Al},t,a_s)$, where x_{Al} is the Al concentration of the $Al_xGa_{1-x}N$ at a depth t, and a_s is the in-plane lattice parameter of the substrate. Using Eqs. (2) and (3) again, we can write the lattice parameter, c_t, of the graded $Al_xGa_{1-x}N$ layers at a depth t as

$$c_t = c_r(x)\left(1 - 2\frac{C_{13}(x)}{C_{33}(x)}\frac{a_s - a_r(x)}{a_r(x)}\right). \tag{4}$$

Thus, knowing a_s and finding the distribution function of c_t allow us to calculate the Al concentration x_{Al} and strain along the graded $Al_xGa_{1-x}N$ layers. This is all predicated on the fact that the in-plane lattice parameter is coherent with the substrate, which is confirmed by an asymmetric reciprocal space map (RSM). Then, by simulation of the symmetric XRD reflection, which would be dependent on only the of out-of-plane lattice parameters, we can determine the composition and thus the strain profiles in the graded $Al_xGa_{1-x}N$ layers.

Since the mosaic crystal model is valid also for graded $Al_xGa_{1-x}N$ layers, and typical thicknesses of layers are thin, we use the kinematical theory of X-ray diffraction to simulate the symmetric reflections.[17] We divided the $Al_xGa_{1-x}N$ film into sub-cells (see Fig. 1), with lattice parameters, c_t, given by Eq. (4) for a varying Al concentration, x_{Al}. Within the limits of this theory, the scattered amplitude of the whole $Al_xGa_{1-x}N$ layer is calculated by summing together the amplitudes from all the unit cells with their own phase factor

$$A(q) = \sum_i F_i \exp(-2\pi i q t_i), \tag{5}$$

where F_i is the structure factor of the cell at depth t_i, and $\boldsymbol{q} = \boldsymbol{k^{in}} - \boldsymbol{k^{out}}$ is the scattering vector ($|\boldsymbol{k^{in}}| = |\boldsymbol{k^{out}}| = |\boldsymbol{k}| = \frac{1}{\lambda}$, where $\boldsymbol{k^{in}}$ and $\boldsymbol{k^{out}}$ are incident and scattered wave vectors). The length of the scattering vector is related to the incidence angle θ given by

$$q = |\boldsymbol{q}| = 2|\boldsymbol{k}|\sin(\theta) = \frac{2\sin(\theta)}{\lambda}. \tag{6}$$

Taking into account Bragg's law and Eq. (1) in Eq. (6), we can determine that the length of the scattering vector perpendicular to the sample surface (q_z) is inversely proportional to the lattice parameter c_t and given by

$$q_z = \frac{n}{d} = \frac{nl}{c_t}. \tag{7}$$

Since the X-ray diffraction experiments can be simply understood using the reciprocal space model, Eqs. (6) and (7) connect the coordinate q_z of reciprocal space with the angular coordinate, θ, in direct space measured with respect to the lattice parameter c_t. Schematically, this is presented in Fig. 1, where we see that for each sub-cell with lattice

[This article is copyrighted as indicated in the article. Reuse of AIP content is subject to the terms at: http://scitation.aip.org/termsconditions. Downloaded to] IP: 193.17.216.226 On: Tue, 16 Dec 2014 12:31:26

parameter c_i the Bragg condition is satisfied only at incidence angle θ_i. Substituting Eq. (6) in Eq. (5), the angular distribution of the scattered intensity, representing the properties of the layer, can be described by its distribution in reciprocal space by

$$I(\theta) = |A(\theta)|^2 e^{-2L} = \left| \sum_i F_i \exp\left(-4\pi i \frac{\sin(\theta)}{\lambda} t_i\right) \right|^2 e^{-2L}, \quad (8)$$

where L is the static Debye-Waller factor.

From Eqs. (6), (7), and (8), we conclude that for homogenous $Al_xGa_{1-x}N$ layer deformation, i.e., $Al_xGa_{1-x}N$ coherently strained to a substrate with $x_{Al} = const$ along the entire layer thickness, the scattered intensity in reciprocal space is shifted proportional to this deformation. The situation is different in the case of inhomogeneous deformation, i.e., graded $Al_xGa_{1-x}N$ with $x_{Al} = f(t)$ coherently strained to a substrate. In Fig. 2, we show examples of simulated symmetric (0002) X-ray diffraction curves changing due to different layer thicknesses, different maximum Al concentration, and different monotonically varying profiles of Al concentration. Here, we assume perfect interfaces between the [0001]-oriented GaN substrate ($a_s = 0.3189$ nm) and the coherently strained, graded $Al_xGa_{1-x}N$ layers. As can be seen, the XRD profiles show typical features such as the Bragg peak of the substrate and layer as well as Kiessig fringes characterizing the sample. Because these fringes are caused by the interference of the waves reflected at the layer surface and at the substrate interface, the period determines the thickness of the layer and their presence indicates the high quality of the interfaces. Indeed, the layer thickness influences mainly the distance between the fringes (Fig. 2(a)), whereas the maximum Al concentration (Fig. 2(b)) and depth profiles (Fig. 2(c)) influence not only the position but also the shape of the diffraction maxima. As a result, the described modelling approach allows for the determination of such parameters as thickness, strain, and composition profile in epitaxial $Al_xGa_{1-x}N$-graded layers by high-resolution x-ray diffraction (HRXRD).

In what follows, we focus our attention, experimentally to graded $Al_xGa_{1-x}N$ layers for which coherent growth on the substrate is the main condition. It should be noted that the graded layers do not necessarily grow coherently to the substrate. Moreover, the question about the mechanism of relaxation and critical thickness of such kind of layers is still open. Independent of the mechanism of strain relaxation, the in-plane lattice parameter can be a constant or can vary over the entire thickness of the film. Nevertheless, the general simulation procedure described above is applicable also for both of these cases. However, for relaxed and quasi-relaxed layers or for layers with varying in-plane lattice parameters, determining the strain and chemical composition would require the measurement of multiple, different RSMs to get precise in-plane lattice parameter information from the film.

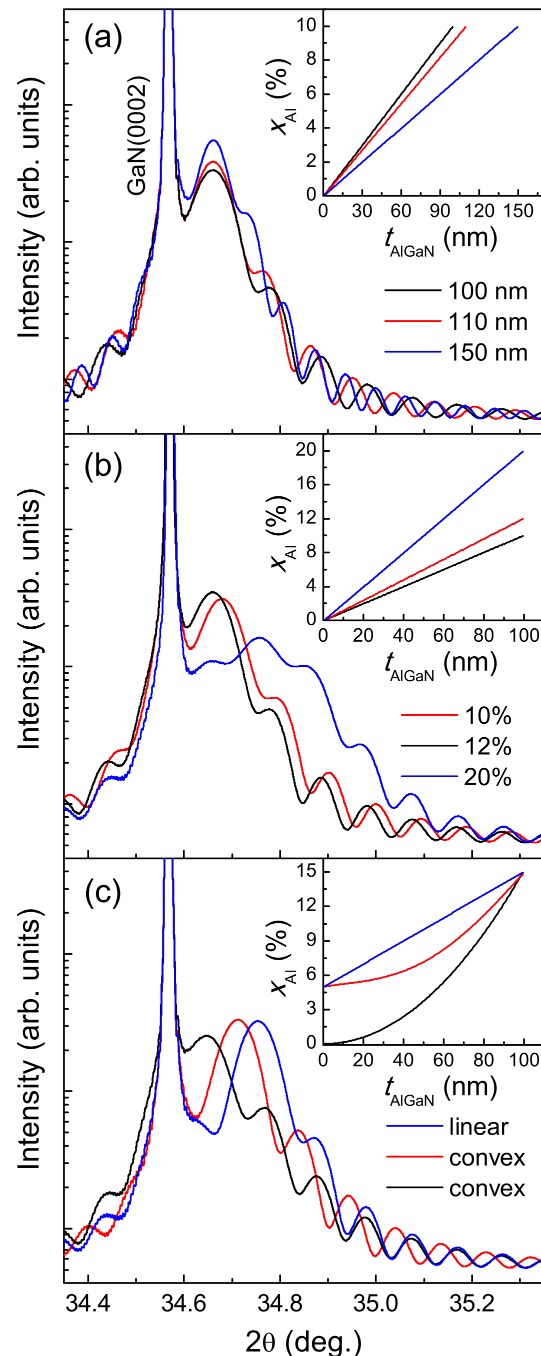

FIG. 2. The calculated symmetric (0002) X-ray diffraction profiles for an $Al_xGa_{1-x}N$ graded layer coherently strained on GaN: (a) the influence of layer thickness; (b) the influence of maximum Al concentration; and (c) the influence of different non-linear Al depth profiles. Insets show the Al depth profiles used for each simulation.

III. EXPERIMENTAL RESULTS

Crystal growth of the $Al_xGa_{1-x}N$ layers studied in this work was performed in a Veeco Gen-II plasma-assisted MBE system. Group III metal was provided by high-purity Ga and Al effusion cells, and active nitrogen was supplied using high-purity gas flowing through a Veeco Unibulb RF plasma source. The samples have been grown on GaN template substrates from KYMA Technologies consisting of ~5 μm of [0001] oriented GaN grown on AlN/sapphire by hydride vapor phase epitaxy (HVPE). The substrates were loaded into ultra-high vacuum and then outgassed at 300 °C in an isolated vacuum chamber. Subsequently, they were moved to the growth chamber and heat cleaned at 700 °C for 1 h in order to remove any residual contamination from both

[This article is copyrighted as indicated in the article. Reuse of AIP content is subject to the terms at: http://scitation.aip.org/termsconditions. Downloaded to] IP: 193.17.216.226 On: Tue, 16 Dec 2014 12:31:26

the surface and the backside titanium coating which is used for heating. Under gallium rich conditions and a substrate temperature of 690 °C, a 240 nm thick Ga-polar, undoped GaN buffer layer was grown after which the RHEED showed a sharp streaky pattern. Following the buffer, the $Al_xGa_{1-x}N$ layers were grown by linearly changing the temperature of the Al effusion cell over 25 min. For sample S1, the cell temperature range was $T_{Al} = 957$–1005.5 °C and for sample S2 it was $T_{Al} = 957$–1026 °C. These ramps should result in layers with Al concentration changing from ∼5% to 20% and 30%, respectively. The substrate temperature for the growth of the graded layer was 710 °C, and the Ga flux used maintains the growth in a metal-rich regime. The nitrogen flow was maintained at 0.5 sccm throughout the growth with a plasma power of 350 W. After growth, all samples were characterized by HRXRD using a Philips X'pert MRD system. We used a standard four-bounce Ge(220) monochromator and three bounce (022) channel cut Ge analyzer crystal along with a 1.6 kW X-ray tube with Cu$K\alpha_1$ radiation and vertical line focus.

In order to estimate the strain state of the layers with respect to the substrate and evaluate their in-plane lattice parameters, first, the asymmetrical (20–25) RSMs were measured. As seen in Fig. 3, for both samples S1 and S2, the intensity of coherent scattering from the GaN substrate and the "tail" from the $Al_xGa_{1-x}N$ layers is distributed in the scattering plane, vertically aligned with each other in q_z direction. This confirms that the growth of the $Al_xGa_{1-x}N$ layers is pseudomorphic, i.e., they are fully strained epitaxial structures with exactly the same in-plane lattice parameter as the substrate ($a_s^{S1} \approx 0.3183$ nm and $a_s^{S2} = 0.3186$ nm). In addition, from the width of the AlGaN tail in the RSMs,[18,19] which is determined by the mosaic spread and lateral coherence length in the film, we conclude that the thin $Al_xGa_{1-x}N$ layers are of high quality. Indeed, the lack of elastic strain relaxation in the $Al_xGa_{1-x}N$ layers testifies that the main source of dislocations is the threading dislocations from the substrate. While there is no reason to expect asymmetrical relaxation in the plane, we measured asymmetrical RSMs also for the (11–24) reflection (not shown here) in order to confirm that the AlGaN film was biaxially pseudomorphic in the plane. The tail from these RSMs was similarly vertically aligned with the substrate. This confirmed a fully strained epitaxial structure for both samples. In principle, the analysis of strain and composition profiles may be based only on the asymmetrical (20–25) RSMs, which has low sensitivity to biaxial strain.[15] However, it is impossible to analyze a q_z scan from the asymmetrical RSM with high precision, because in addition to the strong superposition, the diffracted intensity from the thin graded layers only slightly differs from those of GaN diffuse scattering (see Fig. 3). In view of the fact that thin graded $Al_xGa_{1-x}N$ layers usually grow coherently to the GaN substrate, symmetrical scans are more precise.

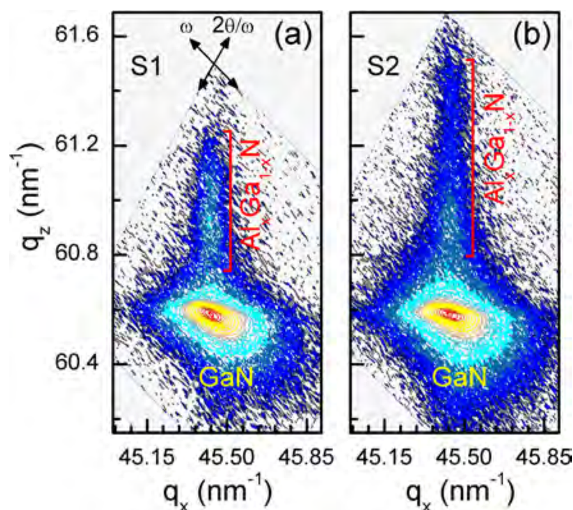

FIG. 3. Asymmetric reciprocal space maps of graded $Al_xGa_{1-x}N$ layer on GaN around the (20–25) reflection for samples S1 (a) and S2 (b). q_z and q_x are the reciprocal space coordinates, which are perpendicular and parallel to the surface, respectively.

Next, we measured the symmetric (0002) RSMs for samples S1 and S2 (Fig. 4, lower panels). The broadening of RSMs in q_x direction (ω-scan) is influenced only by the tilt and finite lateral coherence length of mosaic blocks.[19] For both samples, the full width at half maximum (FWHM) in the q_x direction of the AlGaN tail is similar to if not slightly smaller than the FWHM from GaN including the substrate (template layer). Taking into account the large thickness ratio of the substrate to the layer, we conclude that the structural quality of the $Al_xGa_{1-x}N$ layers is slightly better than the substrate. The length of the tail extending towards the AlN reflection in the q_z direction ($2\theta/\omega$-scan) is governed by the distribution in strain, i.e., the lattice constant, c_t, along the c-axis of the $Al_xGa_{1-x}N$ layers, which is given by the distribution of x_{Al} along the growth direction of the graded $Al_xGa_{1-x}N$ layers using Eq. (4). Thus, the $2\theta/\omega$-scans (Fig. 4, upper panels) were subsequently fit to the simulations taking into account the in-plane lattice parameters of the $Al_xGa_{1-x}N$ graded layers measured from Fig. 3. A multilayer model was used in the fitting procedure with the following layers: (1) GaN substrate; (2) GaN buffer; and (3) graded $Al_xGa_{1-x}N$. We divided the $Al_xGa_{1-x}N$ layer into 175 sub-cells (Fig. 1), with lattice parameters, c_t, given by Eq. (4) for a varying Al concentration, x_{Al}, and used the procedure described in Sec. II. From the simulations, using Eqs. (2)–(4) we calculated the depth profiles of strain and composition, as well as the thickness of the AlGaN-graded layer. Despite the high substrate temperature and a thermally activated exchange mechanism between Al adatoms and Ga surface atoms,[20] we obviously observe fringes on the XRD curve, which indicates a quasi-flat interface. This allows for the precise determination of the thickness of the graded layers of ∼90 ± 2 m, which has been confirmed by transmission electron microscopy. Thus, the deposition rate for both films was found to be ∼3.6 nm/min. This is mainly determined by the active N flux in the metal rich regime. Even though we consider a high incorporation rate of Al,[20] the effect on the layer thickness of the change in alloy concentration is negligible.

The top insets of Figs. 4(a) and 4(b) show the concentration and strain profiles resulting from fitting the symmetric XRD curves of samples S1 and S2, respectively. The Al

[This article is copyrighted as indicated in the article. Reuse of AIP content is subject to the terms at: http://scitation.aip.org/termsconditions. Downloaded to] IP: 193.17.216.226 On: Tue, 16 Dec 2014 12:31:26

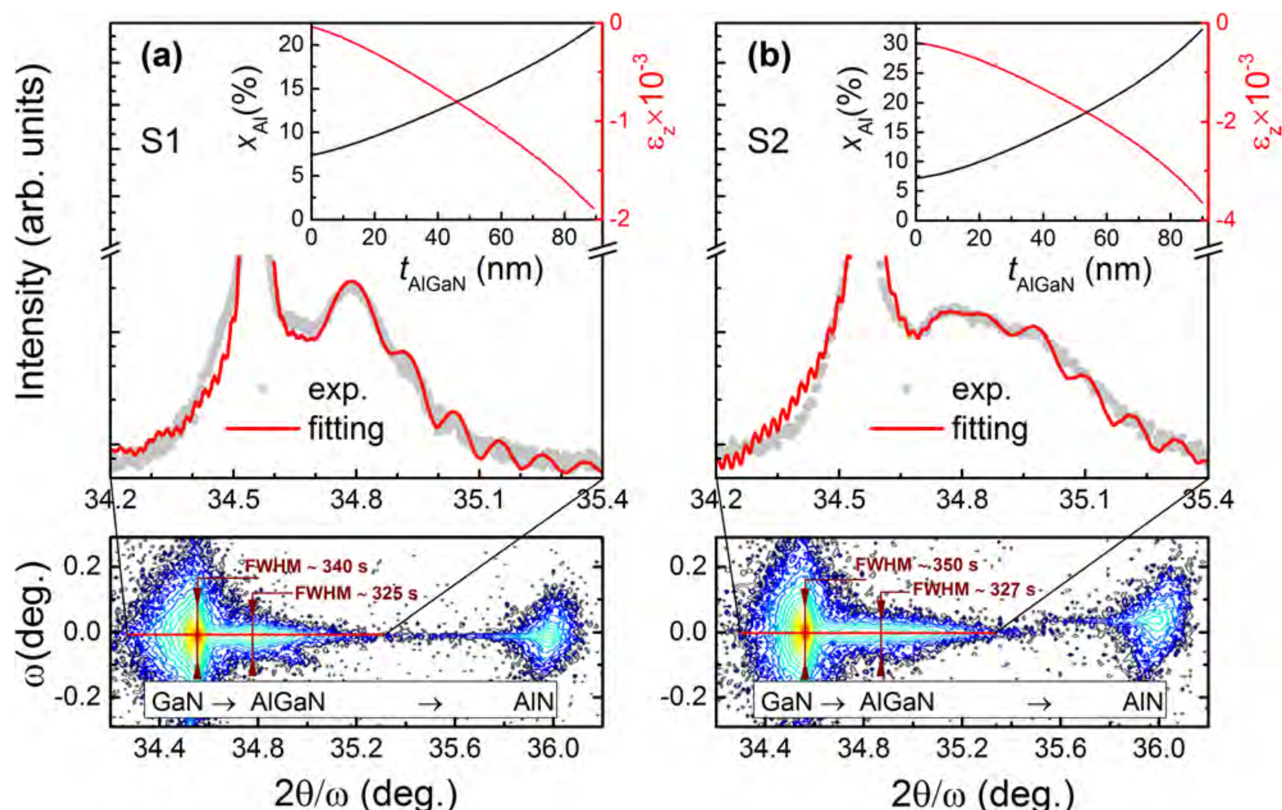

FIG. 4. Experimental (gray line) and calculated (red line) X-ray diffraction profiles, as well as their symmetric (0002) RSMs for samples S1 (a) and S2 (b). The insets present the results of fitting for the concentration and strain distribution as functions of thickness in the graded $Al_xGa_{1-x}N$ layers for each sample.

concentration is $x_{Al} \approx 7\% \rightarrow 22\%$ for sample S1 and $x_{Al} \approx 7\% \rightarrow 32\%$ for sample S2. Through comparative studies to be published elsewhere, we estimate these values to be with $\sim$1% of the true values and are in fact very close to the design parameters for these samples. Moreover, here we see that the Al concentration is not a linear function of depth. This is in fact expected, because the dependence of the Al flux, Φ_{Al}, on the cell temperature, T_{Al}, is Arrhenius-like in nature approximately characterized by the activation energy for evaporating Al from the effusion cell ($\Phi_{Al} \sim \exp(-E_a/k_B T_{Al})$).[2,7,8] This dependence is shown in Fig. 5(a), from which we derive the activation energy of our Al effusion cell to be $\sim$3.3 eV. In order to check for consistency, in addition to samples S1 and S2, we grew four $Al_xGa_{1-x}N$ layers with no grading at different, constant effusion cell temperatures, T_{Al} (constant Al flux Φ_{Al}). Using HRXRD we determined the Al concentration, x^f_{Al}, arriving at the expected linear dependence between x^f_{Al} and Φ_{Al}. This is shown in the inset of Fig. 5(a). Finally, knowing $\Phi_{Al}(T_{Al})$ and $x^f_{Al}(\Phi_{Al})$ we determine the nonlinear function $x^{calib.}_{Al}(T_{Al})$ valid for T_{Al} in the interval from 957 to 1026 °C, which encompasses the temperatures for the growth of our samples. This is shown in Fig. 5(b) by the open circles. This resulting curve is essentially a common calibration of our Al effusion cell for the growth of $Al_xGa_{1-x}N$ based on the four independent growths fixed at different Al concentrations, x^f_{Al}. However, through fitting the XRD from the AlGaN-graded layer samples we arrive at the dependences of $x_{Al}(t_{AlGaN})$ shown in Figs. 4(a) and 4(b). Subsequently, transforming $x_{Al}(t_{AlGaN})$ into $x^{calib.}_{Al}(T_{Al})$ using the linear variation of T_{Al} with time and a fixed growth rate, we obtained an independent calibration of our Al cell for growing $Al_xGa_{1-x}N$ which can, in principle, be based on a single growth. As seen in Fig. 5(b), there is a perfect correspondence between samples S1 and S2 and at the same time an excellent correlation between these two different approaches. It should be noted that for both samples S1 and S2, the Al effusion cell temperatures were ramped with a very low rate <2.7 °C/min, which permits us to compare these two calibration procedures. Because the effusion cell temperature has a finite settling time, in the case of higher ramp rates (thinner graded layers for example), the high-resolution x-ray diffraction is more suitable for calibration. Moreover, application of HRXRD techniques allows us to measure the strain distribution as a function of thickness in the graded $Al_xGa_{1-x}N$ layers. This is important because of the strain induced piezoelectric component of the polarization in the nitrides. Thus, taking into account time dependent instability of fluxes and a finite settling time of temperature of the effusion cells, for growing graded $Al_xGa_{1-x}N$-based structures with pre-defined parameters, the HRXRD can be regarded as a reliable growth calibration technique.

Finally, we want to discuss the new aspect of polarization field engineering used as an attractive doping technique in III–V nitride semiconductors. In previous studies, the polarization-induced doping of different carrier densities results from compositional grading of Al from $x_{Al} = 0 \rightarrow x_{Al} = 10\%–30\%$ (Refs. 1–4) or changing the layer thicknesses while keeping the same compositional grade of Al from $x_{Al} = 0\% \rightarrow x_{Al} = 30\%$.[21] Presented in this work, growth of

[This article is copyrighted as indicated in the article. Reuse of AIP content is subject to the terms at: http://scitation.aip.org/termsconditions. Downloaded to] IP: 193.17.216.226 On: Tue, 16 Dec 2014 12:31:26

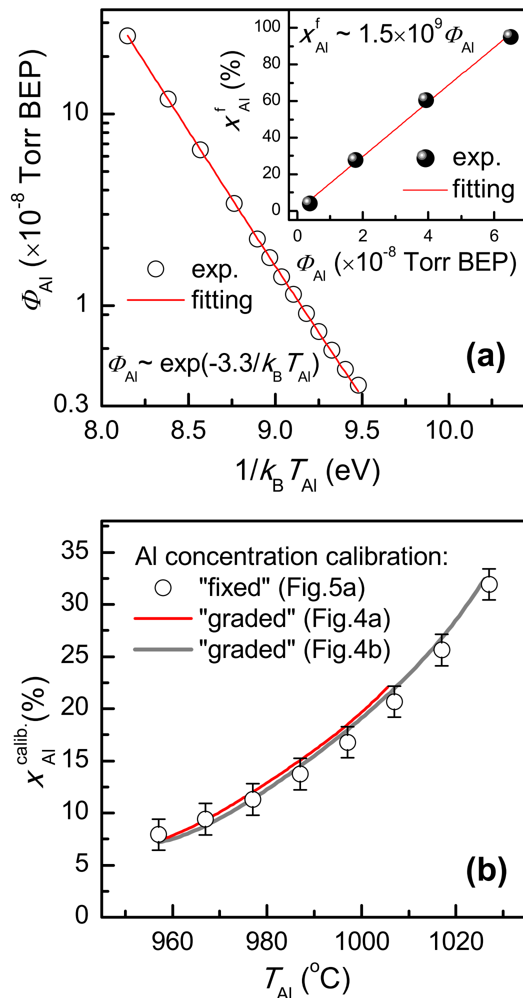

FIG. 5. (a) Experimental Φ_{Al} vs. T_{Al} and x^f_{Al} vs. Φ_{Al} for the effusion cell and MBE used in the present work. The beam equivalent pressure (BEP) of the atomic beam from the Al effusion cell is used to determine Φ_{Al} flux. (b) Calibrated Al effusion cell temperature for the growth of $Al_xGa_{1-x}N$ with a given Al concentration, $x^{calib.}_{Al}$. Open circles represent the results from (a) of comparing beam flux measurements with independent growths with different x^f_{Al} values, and the red and grey curves represent the results of the XRD simulations for samples S1 and S2, respectively.

graded $Al_xGa_{1-x}N$ coherently strained to GaN starting with an Al concentration, $x_{Al} > 0\%$, can be regarded as an additional powerful technique for tuning of the carrier volume density and its confinement in such type of layers.

IV. CONCLUSION

In conclusion, we present a method which allows for the efficient measurement of composition/strain distribution as functions of depth in the graded $Al_xGa_{1-x}N$ layers grown by MBE pseudomorphically on GaN substrates. The method based on a laboratory X-ray diffraction experiment makes use of the asymmetrical RSM covering the full compositional range for epitaxial concentration graded layers of AlGaN and also fitting through kinematical simulations of the intensity profiles ($2\theta/\omega$-scan) of symmetric reflections. Through comparison of these simulations with as-grown samples, we can reliably determine concentration/strain profiles which determine much of the electrical properties of the film. The compositions measured by this method are in good agreement with the standard approach using multiple growth/characterization procedures. Thus, these fitting techniques create opportunities to calibrate growth rates and compositions with a single growth rather than multiple growths as has been done traditionally.

In addition, the experimental results demonstrated here indicate the possibility of growing graded $Al_xGa_{1-x}N$ coherently strained to GaN substrate with starting Al concentrations of $x_{Al} > 0\%$. This creates a new way for tuning the polarization-induced doping carrier densities in graded $Al_xGa_{1-x}N$ layers. This is a topic for our future research.

[1]J. Simon, V. Protasenko, C. Lian, H. Xing, and D. Jena, Science **327**, 60 (2010).
[2]C. Wood and D. Jena, *Polarization Effects in Semiconductors: From Ab-Initio Theory to Device Applications* (Springer Science + Business Media, LLC, New York, 2007).
[3]S. Li, M. Ware, J. Wu, P. Minor, Z. Wang, Z. Wu, Y. Jiang, and G. Salamo, Appl. Phys. Lett. **101**, 122103 (2012).
[4]S. Li, M. Ware, V. Kunets, M. Hawkridge, P. Minor, J. Wu, and G. Salamo, Phys. Status Solidi C **8**(7–8), 2182–2184 (2011).
[5]O. V. Khokhlev, K. A. Bulashevich, and S. Yu. Karpov, Phys. Status Solidi A **210**(7), 1369–1376 (2013).
[6]H. Sun, J. Woodward, J. Yin, A. Moldawer, E. F. Pecora, A. Yu. Nikiforov, L. Negro, and R. Paiella, J. Vac. Sci. Technol., B **31**(3), 03C117 (2013).
[7]J. Verma, S. M. Islam, V. Protasenko, P. K. Kandaswamy, H. Xing, and D. Jena, Appl. Phys. Lett. **104**, 021105 (2014).
[8]S. D. Carnevale, T. F. Kent, P. J. Phillips, M. J. Mills, S. Rajan, and R. C. Myers, Nano Lett. **12**, 915–920 (2012).
[9]S. D. Carnevale, T. F. Kent, P. J. Phillips, A. T. M. G. Sarwar, C. Selcu, R. F. Klie, and R. C. Myers, Nano Lett. **13**, 3029–3035 (2013).
[10]A. Able, W. Wegscheider, K. Engl, and J. Zweck, J. Cryst. Growth **276**, 415–418 (2005).
[11]Y. Yang, P. Xiang, M. Liu, W. Chen, Z. He, X. Han, Y. Ni, F. Yang, Y. Yao, Z. Wu, Y. Liu, and B. Zhang, J. Cryst. Growth **376**, 23–27 (2013).
[12]Y. L. Hsiao, L. C. Lu, C. H. Wu, E. Y. Chang, C. I. Kuo, J. S. Maa, K. L. Lin, T. T. Luong, W. C. Huang, C. H. Chang, C. F. Dee, and B. Y. Majlis, Jpn. J. Appl. Phys., Part 1 **51**, 025505 (2012).
[13]Y. Du, T. C. Droubay, A. V. Liyu, G. Li, and S. A. Chambers, Appl. Phys. Lett. **104**, 163110 (2014).
[14]O. Brandt, P. Waltereit, and K. H. Ploog, J. Phys. D: Appl. Phys. **35**, 577–585 (2002).
[15]D. J. Wallis, D. Zhu, F. Oehler, S. P. Westwater, A. Pujol, and C. J. Humphreys, Semicond. Sci. Technol. **28**, 094006 (2013).
[16]J. Tweedie, R. Collazo, A. Rice, J. Xie, S. Mita, R. Dalmau, and Z. Sitar, J. Appl. Phys. **108**, 043526 (2010).
[17]U. Pietsch, V. Holy, and T. Baumbach, *High-Resolution X-Ray Scattering: From Thin Films to Lateral Nanostructures* (Springer Science + Business Media, LLC, New York, 2004).
[18]V. P. Kladko, A. V. Kuchuk, P. M. Lytvyn, O. M. Yefanov, N. V. Safriuk, A. E. Belyaev, Yu. I. Mazur, E. A. DeCuir, Jr., M. E. Ware, and G. J. Salamo, Nanoscale Res. Lett. **7**, 289 (2012).
[19]M. A. Moram and M. E. Vickers, Rep. Prog. Phys. **72**, 036502 (2009).
[20]A. V. Kuchuk, V. P. Kladko, T. L. Petrenko, V. P. Bryksa, A. E. Belyaev, Yu. I. Mazur, M. E. Ware, E. A. DeCuir, Jr., and G. J. Salamo, Nanotechnology **25**(24), 245602 (2014).
[21]J. Simon, A. Wang, H. Xing, S. Rajan, and D. Jena, Appl. Phys. Lett. **88**, 042109 (2006).

[This article is copyrighted as indicated in the article. Reuse of AIP content is subject to the terms at: http://scitation.aip.org/termsconditions. Downloaded to] IP: 193.17.216.226 On: Tue, 16 Dec 2014 12:31:26